A perturbation-based numerical method for solving a three-dimensional axisymmetric indentation problem

GRIGORIOS A. PAVLIOTIS* and MARK H. HOLMES[†]
Department of Mathematical Sciences, Rensselaer Polytechnic Institute, Troy, NY 12180-3590, USA

Abstract. The three-dimensional axisymmetric problem of the indentation of a thin compressible linear elastic layer bonded to a rigid foundation is considered. Approximate analytical solutions of the problem that incorporate a large portion of the singular deformation gradients near the edge of the indenter are presented. An accurate closed-form expression for the deformation as well as the deformation gradient throughout the layer is provided and its effectiveness in solving the problem numerically is demonstrated. By incorporating the approximate solution into the numerical scheme the accuracy and convergence rate increase dramatically.

Key words: axisymmetric indentation, mechanoreceptors, modified numerical scheme, thin-layer approximation

1. Introduction

Indentation testing is a well-established method for measuring the mechanical properties of materials. The analysis of this testing procedure has a long history [1–10], yet the problem remains of interest. Examples of current applications include nanoindentation testing for thin films [11] hardness studies [12] and biomechanical testing [13].

The indentation problem considered here originally comes from the study of mechanoreceptors in tissue, including Pacinian corpuscles, SA II receptors, and chondrocytes. These receptors, which are generally distributed through the depth of the tissue, are responsible for transducing a component of the deformation field at the receptor location into a neural or chemical signal. In the case of tactile sensors, it is still an open question as to what component of the field is transduced. One hypothesis is that, when using indentation tests to study receptor response, the vertical strain plays a central role in the transduction process [14]. To address this question it is essential to know the deformation throughout the depth and this brings us to the objectives of this paper. In particular, we intend to demonstrate the effectiveness of an analytical approximation of the deformation, both as a relatively simple expression in studying the deformation at the receptor location as well as its effectiveness in producing an accurate numerical method to solve the problem. It is worth mentioning that indentation, using either a flat or spherical end indenter, is used extensively in biological tissue testing. We consider flat-ended indenters since they have the advantage of providing an optimal choice in terms of sensitivity in the indentation test [13].

In this paper we study the three-dimensional axisymmetric static indentation problem. We consider the case of a linear elastic layer bonded to a rigid foundation, with a cylindrical flat-ended rigid indenter. The layer is assumed to be thin, *i.e.* the ratio ϵ of the depth of the
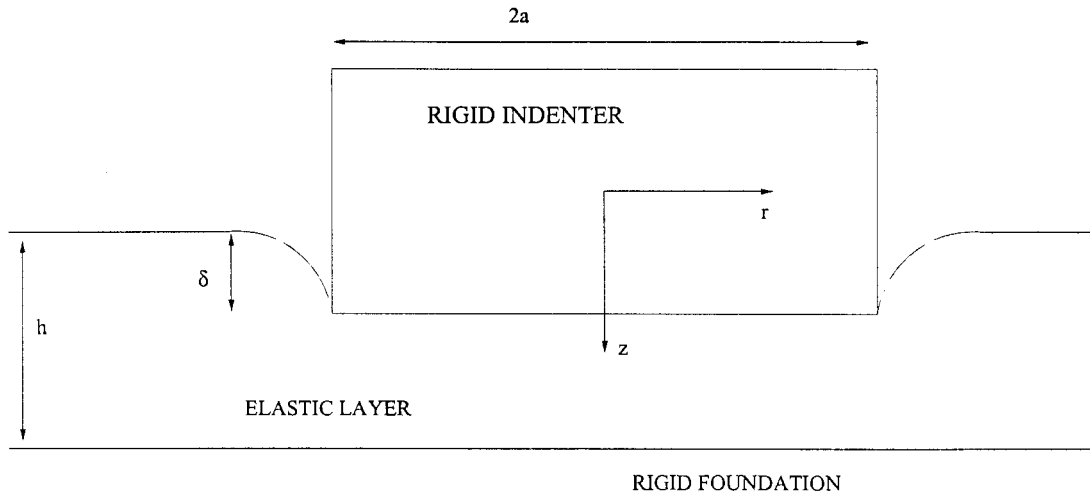
---

*pavlig@rpi.edu
[†]holmes@rpi.edu

Figure 1. Schematic representation of the problem under investigation.

layer h to the radius a of the indenter is taken to be small. The indenter is given a prescribed vertical displacement and is assumed to be frictionless. The resulting mathematical problem is easily expressed as a mixed-boundary-value problem within the linear theory of elasticity ([15], pp. 12–15). Because of the classical nature of the problem numerous approaches have been used to solve it, although most of them are not applicable to our situation. Examples are the classical solutions of Hertz and Boussinesq ([7], pp. 93–98, pp. 204–209), ([16], pp. 76–84) which are valid under the assumption of the layer being thick compared to the radius of the indenter, *i.e.* the limit $h/a >> 1$. The traditional approach to solving the finite-depth problem involves using integral transform techniques ([7, pp. 246–255], [8, 17, 15, 18]. This method requires extensive mathematical analysis to invert the transforms and also has the difficulty that the kernels of the integrals become singular in the limit $\epsilon \rightarrow 0$, ([7, pp. 255–271], [8, 17]. More importantly, these techniques generally provide the deformation field only on the surface of the layer and involve complicated inverse transforms when determining the deformation through the depth.

One might argue, given the complexity of the transform methods, that it would be best to simply solve the problem directly using a numerical method such as finite elements. The complication with this approach, when using a flat-ended indenter, is that the solution is singular at the edge of the indenter and this singularity dominates the response of the layer. What this means is that a direct numerical approach requires extensive refinement in this region and even then it is not clear that an accurate solution is obtained. A much better idea is to incorporate an accurate approximation of the solution, which accounts for this singular behavior, into the numerical algorithm and thereby compute an accurate solution using a much coarser mesh. This will be done in this paper.

In this work we combine approximate analytical solutions that were obtained for the planar problem [19–21], to produce one for the three-dimensional axisymmetric case. We first perform an asymptotic analysis of the problem in terms of the small parameter ϵ to produce an approximate analytical solution. It is shown that the analytical solution obtained in [20, 21] is accurate up to $O(\epsilon)$ for the three-dimensional axisymmetric problem. This solution is compared to the numerical solution found using a finite-difference scheme as well as to an asymptotic approximation derived earlier in [1]. The resulting analytical approximation of

the deformation gradient is also compared to the ones calculated numerically and from the asymptotic solution near the edge of the intender. After this we incorporate the analytical solution into the numerical scheme and we exhibit the fact that the convergence rate and accuracy of the modified scheme is greatly increased.

Our approach to solving the problem has certain advantages. First, it enables us to calculate the deformation field as well as the deformation gradient throughout the layer and not only on the surface. Second, because it is a direct method, the approach has the potential of being extended to nonlinear problems (*i.e.* the case were we assume a nonlinear constitutive relation for the elastic layer) for which the integral-transform techniques do not apply. Moreover, it works efficiently for values of the Poisson ratio that are of practical interest in the study of the mechanical properties of tissue, namely in the range [0·0,0·1], [22].

It should be emphasized that, apart from providing a solution for the axisymmetric indentation problem, the purpose of this paper is to advocate the approach that a combination of analytical and numerical techniques can prove useful for solving efficiently systems of partial differential equations that arise in applications. As such, we believe, the results of the paper are useful not only to researchers in indentation problems but to the general engineering-mathematics community. In fact, one might argue that more sophisticated numerical methods, such as adaptive finite-element or finite-difference schemes could solve this indentation problem at least as effectively as our hybrid numerical/analytical method. However, the methodology that we propose could still be useful within the framework of adaptive numerical methods.

2. Equations of the model

The equilibrium equations of linear elasticity for a homogeneous isotropic body in the absence of body forces are ([23], p. 28):

$$(1 - 2\nu)\Delta\mathbf{u}' + \nabla(\nabla \cdot \mathbf{u}') = \mathbf{0}, \tag{2.1}$$

where $\mathbf{u}'$ is the displacement vector field and ν is the Poisson ratio. In the axisymmetric case, Equation (2.1) becomes:

$$\frac{\partial^2 u'_r}{\partial z'^2} + B\frac{\partial^2 u'_z}{\partial z'\partial r'} + A\frac{\partial}{\partial r'}\left(\frac{1}{r'}\frac{\partial}{\partial r'}(r'u'_r)\right) = 0, \tag{2.2a}$$

$$A\frac{\partial^2 u'_z}{\partial z'^2} + \frac{B}{r'}\frac{\partial^2}{\partial z\partial r'}(r'u'_r) + \frac{1}{r'}\frac{\partial}{\partial r'}\left(r'\frac{\partial u'_z}{\partial r'}\right) = 0, \tag{2.2b}$$

where A and B are constants that depend on the Poisson ratio:

$$A = \frac{2(1 - \nu)}{1 - 2\nu}, \qquad B = \frac{1}{1 - 2\nu}. \tag{2.3}$$

The elastic layer is assumed to be in frictionless contact with the indenter and in bonded contact with a rigid foundation, thus the displacements are taken to be equal to zero at $z = h$. We take the shear stress to be zero over the entire surface. Moreover, the vertical displacement field is assumed to have a prescribed constant initial value, $u_z = \delta$, on the surface underneath the indenter. Consequently, the boundary conditions are:

$$\sigma_{rz} = 0 \qquad \text{for } z' = 0, \quad r' \in [0, \infty), \tag{2.4a}$$

$$\sigma_{zz} = 0 \qquad \text{for } z' = 0, \quad r' \in (a, \infty), \tag{2.4b}$$

$$u'_z = \delta \qquad \text{for } z' = 0, \quad r' \in [0, a], \tag{2.4c}$$

$$u'_z = u'_r = 0 \ \text{for } z' = h, \quad r' \in [0, \infty), \tag{2.4d}$$

where σ is the stress tensor. We want to invoke only the components of the displacement field, hence we rewrite the boundary conditions as:

$$\frac{\partial u'_r}{\partial z'} + \frac{\partial u'_z}{\partial r'} = 0 \qquad \text{for } z' = 0, \quad r' \in [0, \infty), \tag{2.5a}$$

$$(1 - v)\frac{\partial u'_z}{\partial z'} + v(\frac{\partial u'_r}{\partial r'} + \frac{u'_r}{r'}) = 0 \qquad \text{for } z' = 0, \quad r' \in (a, \infty), \tag{2.5b}$$

$$u'_z = \delta \qquad \text{for } z' = 0, \quad r' \in [0, a], \tag{2.5c}$$

$$u'_z = u'_r = 0 \qquad \text{for } z' = h, \quad r' \in [0, \infty), \tag{2.5d}$$

We want to study the case when the elastic layer is thin, *i.e.* the case when the depth of the indenter h is small when compared to the radius of the indenter a. Introducing the dimensionless parameter ϵ,

$$\epsilon \equiv \frac{h}{a} \tag{2.6}$$

we can express the assumption that the layer is thin in the form :

$$\epsilon \ll 1. \tag{2.7}$$

As a first step towards the asymptotic treatment of (2.5) we write it in nondimensional form. To this end, we perform the following change of variables:

$$r = \frac{r'}{a}, \qquad z = \frac{z'}{h}, \qquad \mathbf{u} = \frac{\mathbf{u}'}{\delta}. \tag{2.8}$$

Inserting (2.8) into (2.2) and (2.5) we obtain:

$$\frac{\partial^2 u_r}{\partial z^2} + \epsilon B \frac{\partial^2 u_z}{\partial z \partial r} + \epsilon^2 A \frac{\partial}{\partial r}(\frac{1}{r}\frac{\partial}{\partial r}(r u_r)) = 0, \tag{2.9a}$$

$$A \frac{\partial^2 u_z}{\partial z^2} + \epsilon \frac{B}{r}\frac{\partial^2}{\partial z \partial r}(r u_r) + \epsilon^2 \frac{1}{r}\frac{\partial}{\partial r}(r \frac{\partial u_z}{\partial r}) = 0, \tag{2.9b}$$

$$\frac{\partial u_r}{\partial z} + \epsilon \frac{\partial u_z}{\partial r} = 0 \qquad \text{for } z = 0, \quad r \in [0, \infty), \tag{2.9c}$$

$$(1 - v)\frac{\partial u_z}{\partial z} + \epsilon v(\frac{\partial u_r}{\partial r} + \frac{u_r}{r}) = 0 \qquad \text{for } z = 0, \quad r \in (1, \infty), \tag{2.9d}$$

$$u_z = 1 \qquad \text{for } z = 0, \quad r \in [0, 1], \tag{2.9e}$$

$$u_z = u_r = 0 \qquad \text{for } z = 1, \quad r \in [0, \infty). \tag{2.9f}$$

3. Asymptotic analysis - Approximate solutions

We use the fact that the parameter ϵ is small in order to develop asymptotic approximations for the components of the deformation field. Substituting first-order expansions of the form

$$u_r = u_r^{(0)} + O(\epsilon), \tag{3.10}$$

$$u_z = u_z^{(0)} + O(\epsilon) \tag{3.11}$$

in (2.9) we obtain the outer solution [21]:

$$u_r^{(0)} = 0, \tag{3.12}$$

$$u_z^{(0)} = \begin{cases} 1 - z & \text{for} : 0 \leq r < 1 \\ 0 & \text{for} : 1 < r < \infty \end{cases}.$$

In order to solve the interior-layer problem we first introduce the transition-layer coordinates:

$$R \equiv \frac{r-1}{\epsilon}, \qquad z \equiv z \qquad \mathbf{U}(R, z) \equiv \mathbf{u}(r, z). \tag{3.13}$$

The boundary-value problem (2.9), expressed in the transition layer coordinates, becomes:

$$\frac{\partial^2 U_R}{\partial z^2} + B\frac{\partial^2 U_z}{\partial z \partial R} + A\frac{\partial}{\partial R}\left(\frac{1}{1+\epsilon R}\frac{\partial}{\partial R}((1+\epsilon R)U_R)\right) = 0, \tag{3.14a}$$

$$A\frac{\partial^2 U_z}{\partial z^2} + \frac{B}{1+\epsilon R}\frac{\partial}{\partial R}\left((1+\epsilon R)\frac{\partial U_R}{\partial z}\right) + \frac{1}{1+\epsilon R}\frac{\partial}{\partial R}\left((1+\epsilon R)\frac{\partial U_z}{\partial R}\right) = 0, \tag{3.14b}$$

$$\frac{\partial U_R}{\partial z} + \frac{\partial U_z}{\partial R} = 0 \qquad \text{for } z = 0, \quad R \in [-\frac{1}{\epsilon}, 0], \tag{3.14c}$$

$$(1-v)\frac{\partial U_z}{\partial z} + \epsilon v\frac{\partial U_R}{\partial R} + \frac{v}{1+\epsilon R}U_R = 0 \qquad \text{for } z = 0, \quad R \in (0, \infty), \tag{3.14d}$$

$$U_z = 1 \qquad \text{for } z = 0, \quad R \in [-\frac{1}{\epsilon}, 0], \tag{3.14e}$$

$$U_z = U_R = 0 \qquad \text{for } z = 1, \quad R \in [-\frac{1}{\epsilon}, \infty). \tag{3.14f}$$

Inserting asymptotic expansions for the deformation field of the form

$$\mathbf{U} = \mathbf{U}^0 + O(\epsilon) \tag{3.15}$$

in (3.14) and letting $\epsilon \to 0$ we obtain the following BVP for the deformation field in the transition layer:

$$\frac{\partial^2 U^0{}_R}{\partial z^2} + B\frac{\partial^2 U^0{}_z}{\partial z \partial R} + A\frac{\partial^2 U^0{}_z}{\partial R^2} = 0, \tag{3.16a}$$

$$A\frac{\partial^2 U^0{}_z}{\partial z^2} + B\frac{\partial^2 U^0{}_R}{\partial R \partial z} + \frac{\partial^2 U^0{}_z}{\partial R^2} = 0, \tag{3.16b}$$

$$\frac{\partial U^0{}_R}{\partial z} + \frac{\partial U^0{}_z}{\partial R} = 0 \qquad \text{for } z = 0, \quad R \in (-\infty, \infty), \tag{3.16c}$$

$$(1 - \nu)\frac{\partial U^0{}_z}{\partial z} + \nu\frac{\partial U^0{}_R}{\partial R} = 0 \qquad \text{for } z = 0, \quad R \in (0, \infty), \tag{3.16d}$$

$$U^0{}_z = 1 \qquad \text{for } z = 0, \quad R \in (-\infty, 0), \tag{3.16e}$$

$$U^0{}_z = 0 \qquad \text{for } z = 1, \quad R \in (-\infty, \infty), \tag{3.16f}$$

$$U^0{}_R = 0 \qquad \text{for } z = 1, \quad R \in (-\infty, \infty). \tag{3.16g}$$

The $O(1)$ inner axisymmetric problem is the same as the planar inner problem. Thus, we can use the approximate analytical solutions obtained in [21] to derive a first-order approximation for the inner axisymmetric problem. The BVP (3.16) was solved approximately in [21] using the Papkovich-Neuber representation that involves two harmonic potential functions $\psi(R, z)$, $\phi(R, z)$. A BVP for Laplace's equation was then solved for the two potential functions using conformal mapping and calculating the appropriate Green's function. The deformation field resulting from the two potential functions satisfies the equilibrium equations and all but two of the boundary conditions, namely (3.16c), (3.16g). It was argued that, since the objective was to obtain analytical expressions that incorporate a large portion of the singularity in the solution, only the 'essential' boundary conditions that are responsible for the formation of the singularity are important. We shall see, by comparing the analytical expressions with the numerical solution as well as with a well known asymptotic solution, that the formula obtained for the vertical deformation field is in close agreement with the actual solution. The approximate expressions for the first-order displacement fields are [20, 21]:

$$U_R(R, z) = \frac{c_1 z}{\sqrt{2}} \frac{\sqrt{f_1(R, z) + f_2(R, z)}}{f_1(R, z)} - \int_1^z H(R, s, z)\,ds$$
$$+ \frac{1 - (3 - 4\nu)c_1}{\pi} \log\left(\frac{\sqrt{e^{\pi R} + 1} - 1}{\sqrt{e^{\pi R} + 1} + 1}\right) + \frac{c_1 R}{\sqrt{e^{\pi R} + 1}}, \tag{3.17a}$$

$$U_z(R, z) = \frac{1}{\pi}\text{atan}\left(\frac{\sqrt{2}\sqrt{f_1(R, z) + f_2(R, z)}}{f_1(R, z) - 1}\right)$$
$$- \frac{c_1 R}{\sqrt{2}} \frac{e^{\pi R}\sin \pi z}{f_1(R, z)\sqrt{f_1(R, z) - f_2(R, z)}}, \tag{3.17b}$$

where :

$$c_1 = \frac{2}{3 - 4\nu}, \tag{3.18a}$$

$$H(R, s, z) = \frac{1 - (2 - 4\nu)c_1}{\sqrt{2}} \frac{\sqrt{f_1(R, s) + f_2(R, s)}}{f_1(R, s)}$$
$$- \frac{\pi c_1}{2\sqrt{2}} \frac{R(f_1(R, s)g_2(R, s) + g_1(R, s))}{\sqrt{f_1(R, s) + f_2(R, s)}\,f_1(R, s)^3}$$
$$- \frac{\pi c_1}{2\sqrt{2}} \frac{z(f_1(R, s)g_2(R, s) - g_1(R, s)}{\sqrt{f_1(R, s) - f_2(R, s)}\,f_1(R, s)^3}, \tag{3.18b}$$

$$f_1(R, s) = \sqrt{e^{2\pi R} + 1 - 2e^{\pi R} \cos \pi s}, \tag{3.18c}$$

$$f_2(R, s) = e^{\pi R} \cos \pi s - 1, \tag{3.18d}$$

$$g_1(R, s) = e^{3\pi R} \cos \pi s + e^{\pi R} \cos \pi s - 2e^{2\pi R}, \tag{3.18e}$$

$$g_2(R, s) = e^{2\pi R} - e^{\pi R} \cos \pi s. \tag{3.18f}$$

The function atan is defined in terms of the principal branch Atan as :

$$\text{atan}(\omega) = \begin{cases} \text{Atan}(\omega) & \omega \geq 0 \\ \text{Atan}(\omega) + \pi & \omega < 0 \end{cases}.$$

From the assumptions under which these formulas were obtained it is to be expected that only the expression for the vertical component of the deformation field will be in close agreement with the actual solution. Indeed, the expression for u_r does not match with the outer solution. This is not an issue in what follows as the vertical deformation is of primary interest. It is possible to adapt the analysis to derive a similar approximation for u_r but this will be left for future study.

The analytical expression for the vertical component of the deformation field enables us to obtain an approximation for the normal stress field as well as the applied normal pressure. Indeed, from the formula

$$\sigma_{zz} = \frac{2\mu}{1 - 2\nu} \left[(1 - \nu) \frac{\partial u_z}{\partial z} + \epsilon \nu \left(\frac{\partial u_r}{\partial r} + \frac{1}{r} u_r \right) \right], \tag{3.19}$$

where μ is the apparent shear modulus, we see that to $O(1)$, σ_{zz} depends only on u_z. The dimensionless applied load can be obtained upon integration of the surface normal stress :

$$P = \left(\frac{4\mu a \delta}{1 - \nu} \right)^{-1} 2\pi \int_0^a \sigma_{zz}|_{z=0} \, r \, \mathrm{d}r. \tag{3.20}$$

With the derivation of the approximate solution completed, we will turn to questions related to its accuracy and usefulness to provide information about the deformation in the layer. Unfortunately, however, there are no exact solutions to compare with. For this reason the next step will be the development and analysis of a numerical solution which can serve as a basis for comparison.

4. Results

4.1. NUMERICAL SOLUTION

We solve the BVP (2.9) numerically using finite differences. We discretize the domain using a uniform mesh with $2M + 1$ and N nodes in the r and z direction, respectively. Because of the singularity, the mesh has a node placed at the edge of the indenter, $r = 1$, $z = 0$.

We use second-order accurate finite differences throughout the computational domain and the boundaries. We use one-sided first-order-accurate finite differences only when approximating $\partial u_r / \partial z$, $\partial u_z / \partial z$ at $z = 0$. Moreover, we use one-sided differences to approximate $\partial u_r / \partial r$ in the boundary condition (2.9c) at $r = 1$, $z = 0$, since only the left-side derivative exists there. Another possibility would be to use second-order finite differences to approximate

the partial derivatives on the boundary. However, since the gradient of the displacement field becomes singular at the edge of the intender, a higher-order finite-difference approximation of the displacement gradient would be a poor choice in that region. Moreover, as will be seen in the solutions shown later, the displacement gradients on the surface vanish rapidly away from the singularity, so using a higher-order approximation would not significantly improve the accuracy of the numerical scheme in that region. Moreover, as one can see from Figure 10 the convergence rate of the numerical scheme is quadratic, so the approximation of the gradients with first-order differences does not reduce the convergence rate of the numerical solution.

We calculate the numerical solution in the domain $\Omega \equiv (r \in [0, 2], z \in [0, 1])$. This choice was justified after a series of numerical tests in different domains that exhibited the fact that the solution is effectively zero outside the computational domain $\Omega \equiv (r \in [0, r_f], z \in [0, 1])$ for $r_f > 1 \cdot 5$ and $\epsilon < 0 \cdot 3$. We specify boundary conditions at $r = 0$, $r = 2$ using the outer solution.

The discretization procedure results in an asymmetric sparse linear system of equations. We solve it using the bi-conjugate gradient method with incomplete LU factorization for preconditioning. The iteration procedure was terminated when a relative accuracy criterion with tolerance 10^{-7} was satisfied. We used the F11BAF-F11BBF-F11BCF NAG routines.

In Figures 2 and 3 we present the components of the deformation field at various depths for $\epsilon = 0 \cdot 1$ and $\nu = 0 \cdot 1$, $\epsilon = 0 \cdot 1$ and $\nu = 0 \cdot 0$, respectively. We use 3201 and 800 points on the radial and vertical directions, respectively. We see that the singularity in the gradients disappears as we move towards the interior. In fact, in accordance with the theory of elliptic equations, the solution is infinitely smooth throughout the interior of the layer ([24, pp. 308– 326]. We also observe the localized nature of the singularity at $r = 1$, $z = 0$, as well as the interior layer structure of the solution near $r = 1$. This fact also justifies our choice of solving the problem in the computational domain Ω defined in the previous paragraph, since both the vertical and the horizontal displacement fields vanish outside this region. By comparing between the horizontal components of the deformation field for $\nu = 0 \cdot 1$ and $\nu = 0 \cdot 0$ we see that the strength of the singularity at $r = 1$, $z = 0$ increases as the Poisson ratio decreases. Moreover, although it is not shown in these figures, the strength of the singularity increases as ϵ decreases.

In Figures 4 and 5 we present the deformation field throughout the layer. This complements the curves in Figure 3. We use the same mesh as before. We observe that there is a region with a slight outward deformation. This is also apparent in Figures 2 and 3 deformation decreases as ν decreases.

4.2. Modified numerical scheme

From the numerical results that we have presented so far it is clear that the reason we have to use a fine mesh in order to solve the boundary value problem numerically is the presence of the singularity in the gradients on the surface at the edge of the indenter. On the other hand, the approximate analytical solutions, at least for the vertical deformation field, incorporate a large portion of the singularity. Thus, we can use the analytical solutions in order to obtain a BVP that is 'less singular' and thus have a problem that can be solved accurately using a coarser mesh. In other words, we want to subtract the analytical solutions from the original BVP and solve the resulting problem for the residual deformation fields. To this end, we write the components of the displacement field as
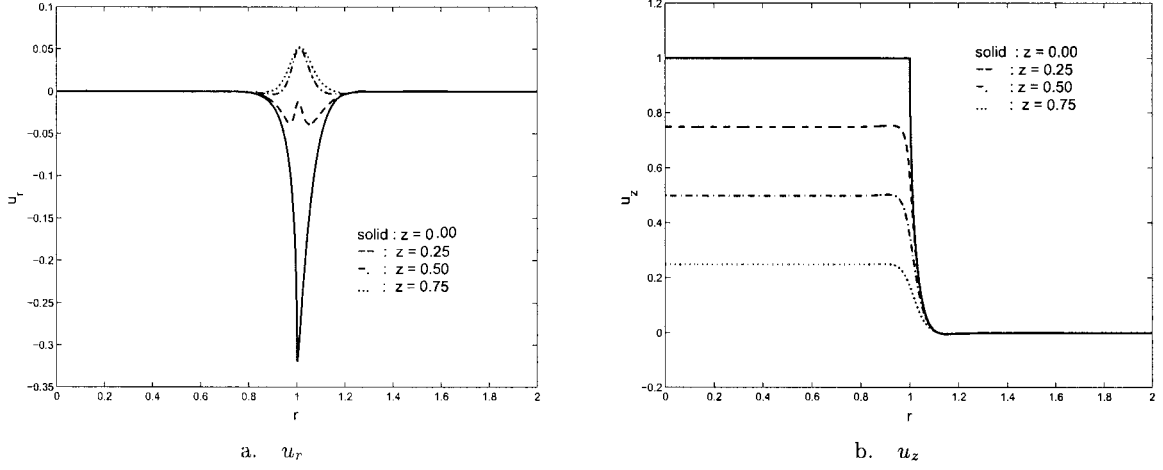
$$u_z = u_z^a + u_z^r, \qquad (4.21a)$$

a. u_r b. u_z

Figure 2. Numerically calculated displacement field for $\epsilon = 0{\cdot}1$, $\nu = 0{\cdot}1$. Mesh points: $M = 3201$ in the radial direction, $N = 800$ in the vertical direction.
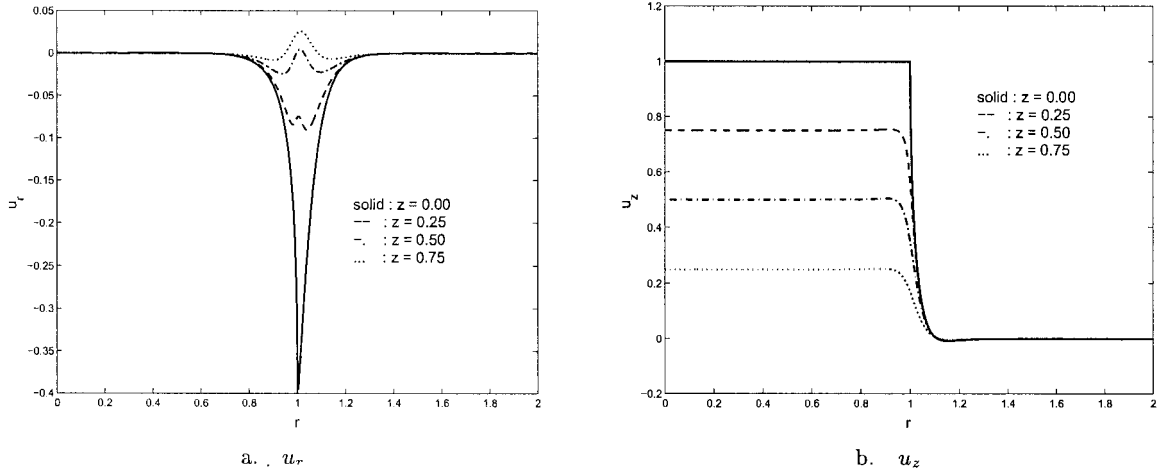

a. . u_r b. u_z

Figure 3. Numerically calculated displacement field for $\epsilon = 0{\cdot}1$, $\nu = 0{\cdot}0$. Mesh points: $M = 3201$ in the radial direction, $N = 800$ in the vertical direction.

$$u_z = u_r^a + u_r^r, \tag{4.21b}$$

where u_z^a, u_r^a are the analytical solutions (3.17a), (3.17b). The components of the residual deformation field u_z^r, u_r^r satisfy the following inhomogeneous BVP:

$$\frac{\partial^2 u_r^r}{\partial z^2} + \epsilon B \frac{\partial^2 u_z^r}{\partial z \partial r} + \epsilon^2 A \frac{\partial}{\partial r}(\frac{1}{r}\frac{\partial}{\partial r}(r u_r^r)) = h_1(r, z), \tag{4.22a}$$

$$A \frac{\partial^2 u_z^r}{\partial z^2} + \epsilon \frac{B}{r}\frac{\partial^2}{\partial z \partial r}(r u_r^r) + \epsilon^2 \frac{1}{r}\frac{\partial}{\partial r}(r \frac{\partial u_z^r}{\partial r}) = h_2(r, z), \tag{4.22b}$$

$$\frac{\partial u_r^r}{\partial z} + \epsilon \frac{\partial u_z^r}{\partial r} = h_3(r) \qquad \text{for } z = 0, \quad r \in [0, \infty), \tag{4.22c}$$
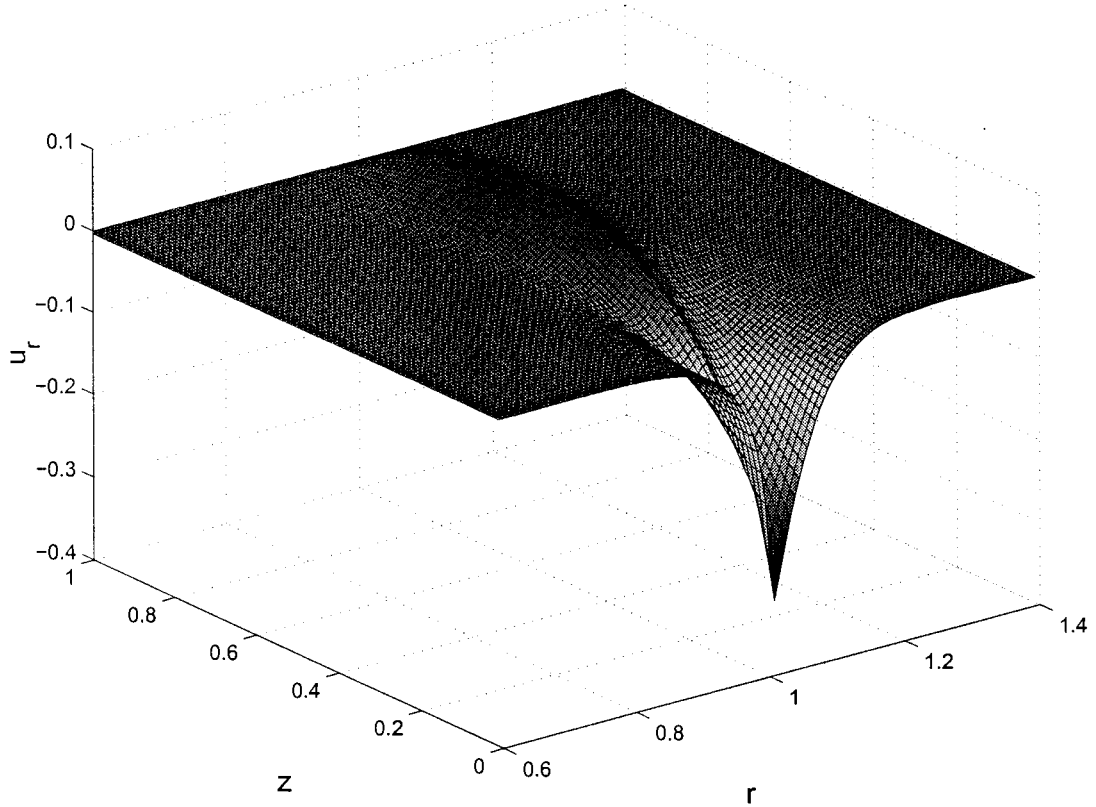
Figure 4. Numerically calculated horizontal component of the deformation field throughout the layer for $\epsilon = 0{\cdot}1$, $\nu = 0{\cdot}0$.

$$(1 - \nu)\frac{\partial u_z^r}{\partial z} + \epsilon\nu(\frac{\partial u_r^r}{\partial r} + \frac{u_r^r}{r}) = h_4(r) \qquad \text{for} \qquad z = 0, \quad r \in (1, \infty), \tag{4.22d}$$

$$u_z^r = 0 \qquad \text{for } z = 0, \quad r \in [0, 1], \tag{4.22e}$$

$$u_z^r = u_r^r = 0 \qquad \text{for } z = 1, \quad r \in [0, \infty), \tag{4.22f}$$

where the inhomogeneous terms h_1, h_2, h_3, h_4 are obtained by applying the differential operators that appear on the left-hand side of the equations to u_r^a, u_z^a. The integrals required for the evaluation of the right hand side of (4.22) are calculated using a composite Simpson's rule.

4.3. COMPARISONS

Our goal in this section is twofold: we wish to assess the validity of the analytical solution for the vertical component of the deformation field by comparing it with the numerical solution as well as a well known asymptotic solution. Moreover, we wish to exhibit the fact that the modified numerical scheme converges significantly faster than the original one.

Alblas and Kuipers in [1] obtained, using the Wiener- Hopf technique, an asymptotic solution valid in the immediate vicinity of the edge of the indenter. This result was obtained for the planar problem but is valid for the axisymmetric problem as well, with the same accuracy. Their approximation is:
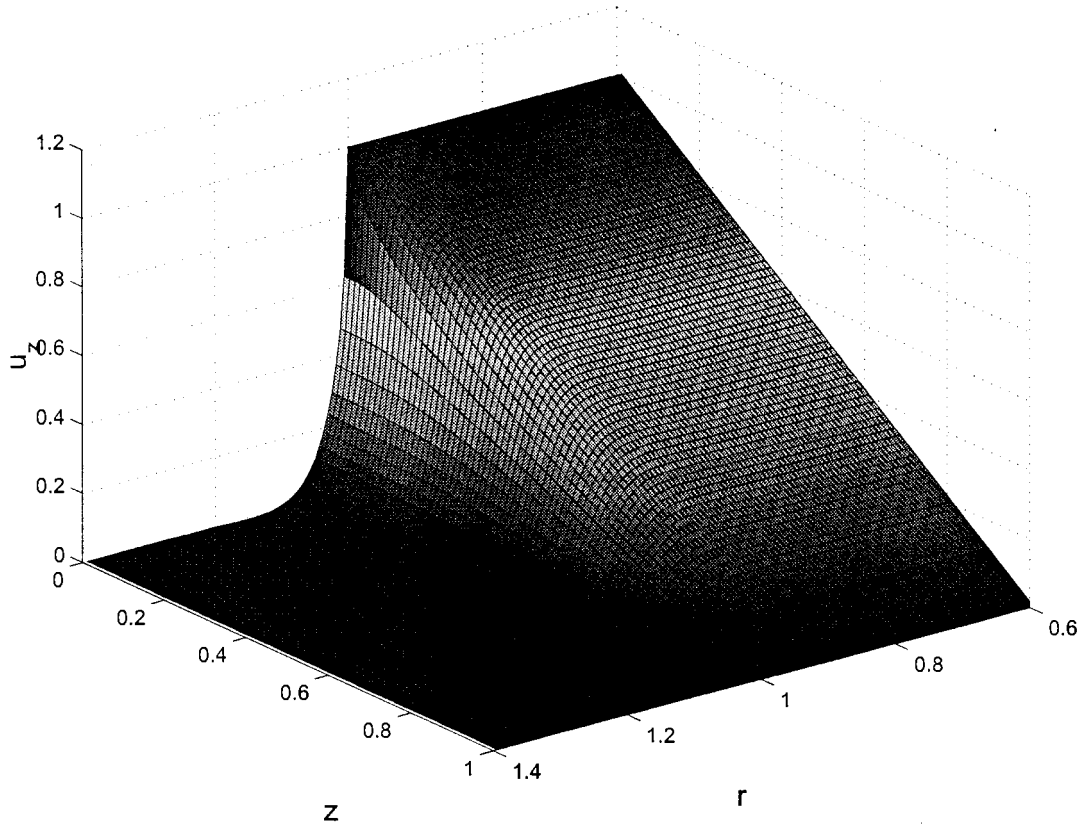
Figure 5. Numerically calculated vertical component of the deformation field throughout the layer for $\epsilon = 0{\cdot}1$, $\nu = 0{\cdot}0$.

$$u_z(r, 0) \approx 1 - \frac{2}{\sqrt{\pi}} \sqrt{\frac{2(1-\nu)^2}{1-2\nu}} \sqrt{\frac{r-1}{\epsilon}}, \tag{4.23}$$

which is valid for $0 < r - 1 << 1$, $\nu \in [0, 0{\cdot}5)$.

In Figure 6 we compare between the analytical approximation (3.17b), the asymptotic solution (Alblas-Kuipers) and the numerical solution obtained in two different meshes, one coarser and one finer. We observe that near the edge of the indenter the numerical solution, as we refine the mesh, converges to the asymptotic and the analytical solutions. This justifies the conclusion that the analytical approximation provides us with a very accurate approximation of the solution, at least near the edge of the indenter. It also demonstrates the difficulty the numerical solution has in resolving the singularity and the necessity of a very fine mesh in this region.

In Figure 9 we compare the analytical approximation and the numerical solution obtained using the finest mesh. We see again that the analytical solution is accurate over the surface except for a small region somewhat pass the edge of the indenter.

A natural question to ask is whether the approximate analytical solution provides us with an accurate description of the gradient of the displacement fields. This issue is addressed in Figure 7 where we compare between the derivative of the vertical component of the displacement field along the horizontal direction $\partial u_z / \partial r$ near the edge of the indenter obtained from the numerical solution, the approximate analytical solution and the Alblas-Kuipers solution.
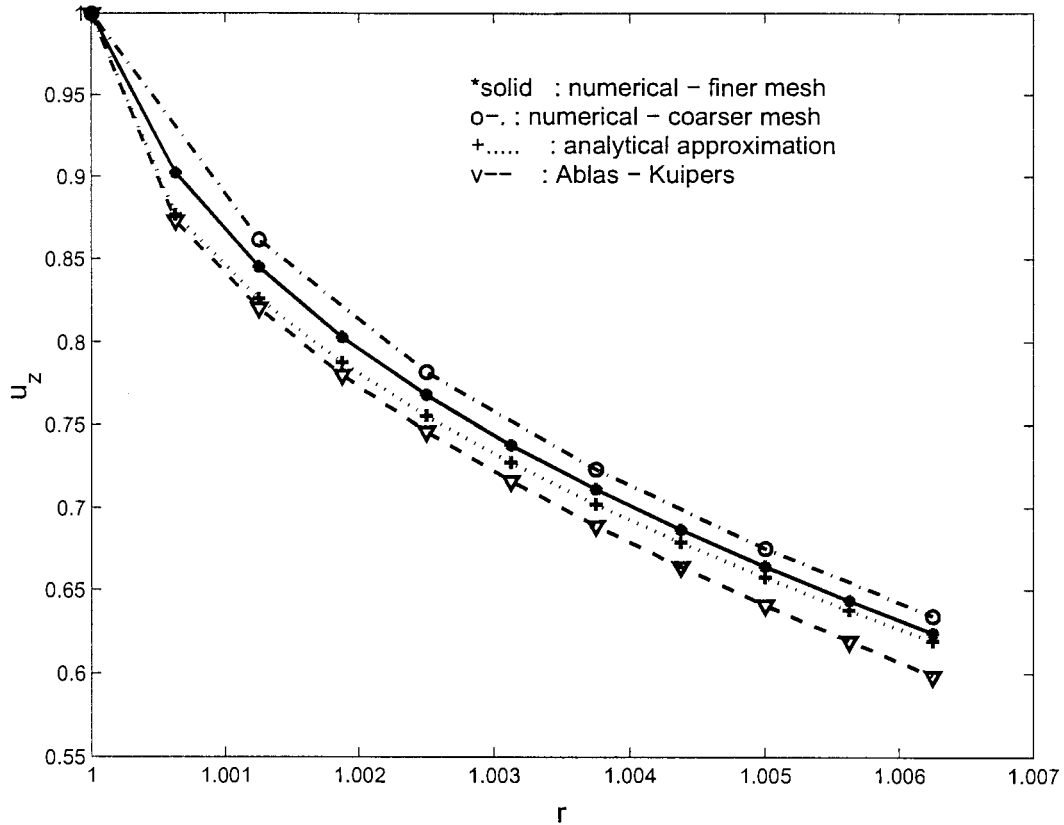
Figure 6. Comparison between numerical, analytical and asymptotic solutions for u_z at $z = 0$ near $r = 1$, $\epsilon = 0.1$, $\nu = 0.1$.

We see that the agreement between the numerically calculated gradient and the one obtained through differentiation of (3.17b) for $z = 0$ is remarkable. On the other hand, the displacement gradient calculated from the Ablas-Kuipers solution provides an accurate description of the gradient only very near $z = 0, r = 1$ and, moreover, the accuracy diminishes as we move away from the edge of the intender, as expected. Moreover, in Figure 8 we compare between the numerical and analytical approximation as well as the gradients along the horizontal direction at $z = 0.25$. Again the conclusion is that (3.17b) provides us with a very accurate description of both u_z as well as $\partial u_z / \partial r$ throughout the layer.

We now wish to justify the fact that the convergence rate of the modified numerical scheme is higher than that of the original scheme when solving for the vertical component of the deformation field. We solve the problem using various meshes and we take the solution obtained with the original scheme using the finest mesh to be the exact solution. We use $2M + 1$ points on the radial direction and $N = \frac{1}{2}M$ in the vertical direction, where M varies from 200 to 1600.

To investigate the relative improvement of the computed solution as the mesh is refined we need a measure for the 'error' of the solutions obtained. As seen in Figures 2 and 3, the elliptic nature of the problem results in a smooth solution throughout the interior of the layer $(0 < z \le 1)$. Consequently, the most computationally difficult component of the displacement field to compute accurately occurs on the surface $(z = 0)$. To measure the error we will use
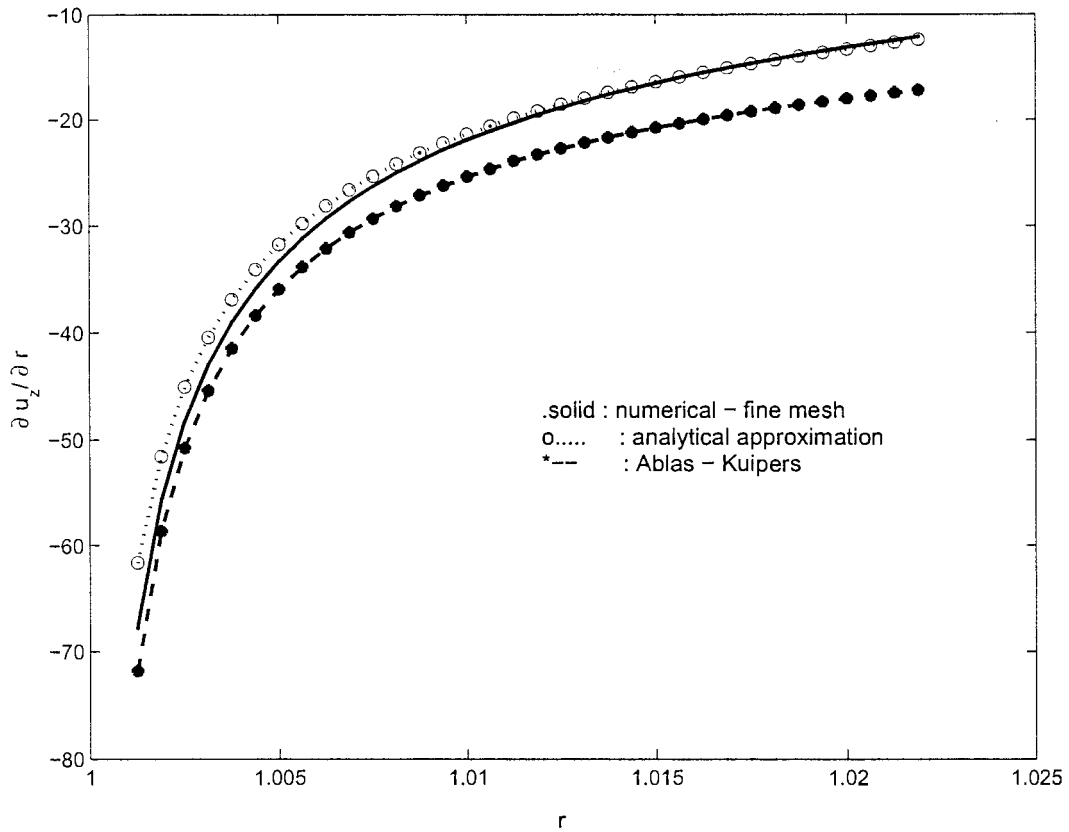
Figure 7. Comparison between numerical, analytical and asymptotic solutions for $\partial u_z/\partial r$ at $z = 0$ near $r = 1$, $\epsilon = 0\cdot1$, $v = 0\cdot1$.
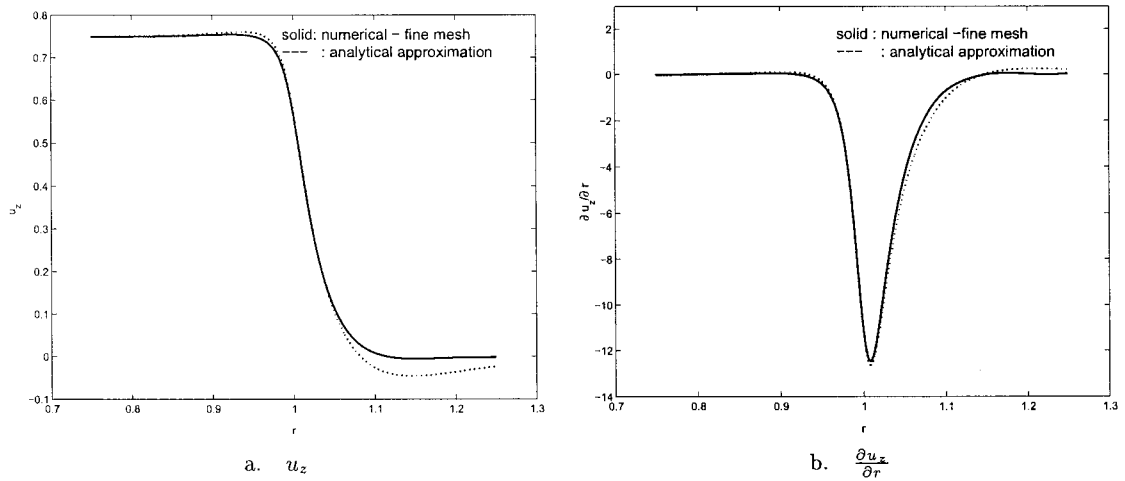

Figure 8. Comparison between numerical and analytical solutions for u_z and $\partial u_z/\partial r$ at $z = 0\cdot25$ for $\epsilon = 0\cdot1$, $v = 0\cdot1$.
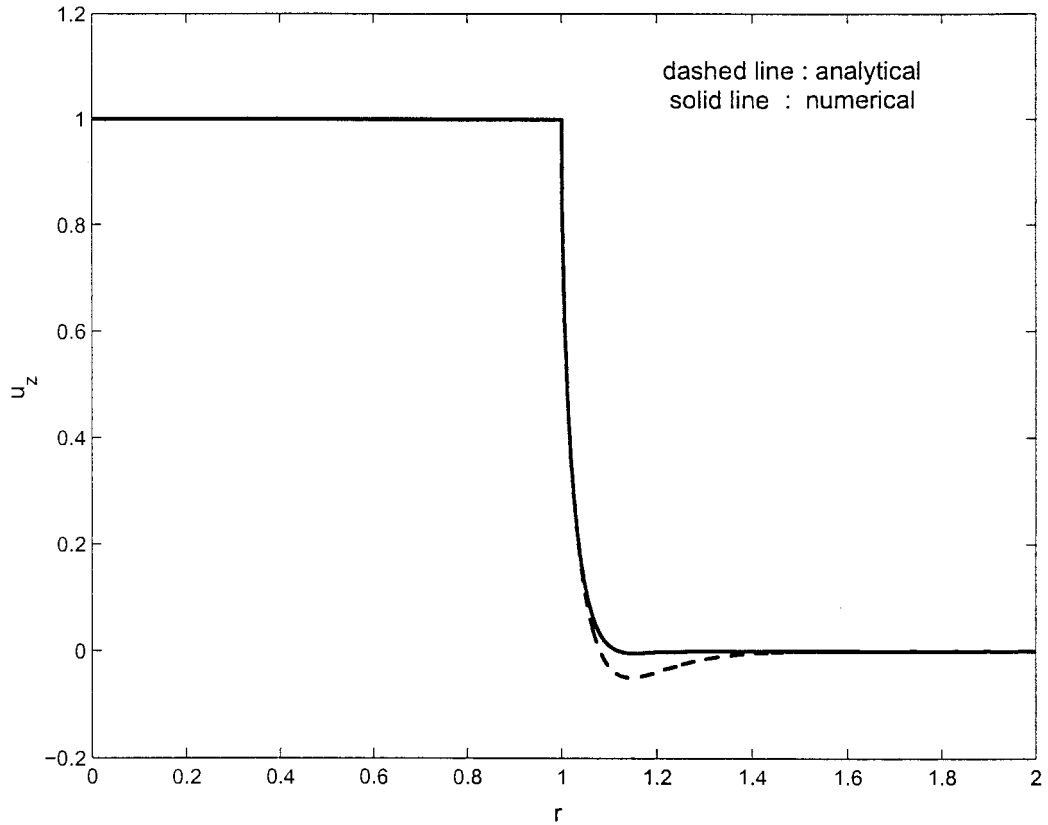
Figure 9. Comparison between the numerical and the analytical solution for u_z at $z = 0$, for $\epsilon = 0 \cdot 1$, $\nu = 0 \cdot 1$.

the integrated radial displacement under the indenter ($0 \leq r \leq 1$). In particular, as a measure of the error between the 'exact' solution u_r and the numerical solution $\tilde{u}_r$ we use:

$$
\begin{aligned}
||e|| &= | \int_0^1 |u(r, 0)| \, r \, \mathrm{d}r - \int_0^1 |\tilde{u}(r, 0)| \, r \, \mathrm{d}r | \\
&= \int_0^1 |u(r, 0) - \tilde{u}(r, 0)| \, r \, \mathrm{d}r,
\end{aligned}
\tag{4.24}
$$

The reason for the above equality is the fact that the radial component of the displacement field is negative on this interval (see Figures 2 and 3). The integrals in (4.24) are calculated numerically using a composite Simpson's rule.

In the figures presented so far we have been using the original numerical scheme. We compare between the convergence rates of the two schemes in Figure 10. We readily see that the convergence rate for the vertical deformation using the modified scheme is much higher. In terms of CPU time, the numerical solution using the finest mesh and the original scheme was obtained in 23·673 sec, whereas the modified scheme provided us with the same accuracy in 2·041 sec using a much coarser mesh.
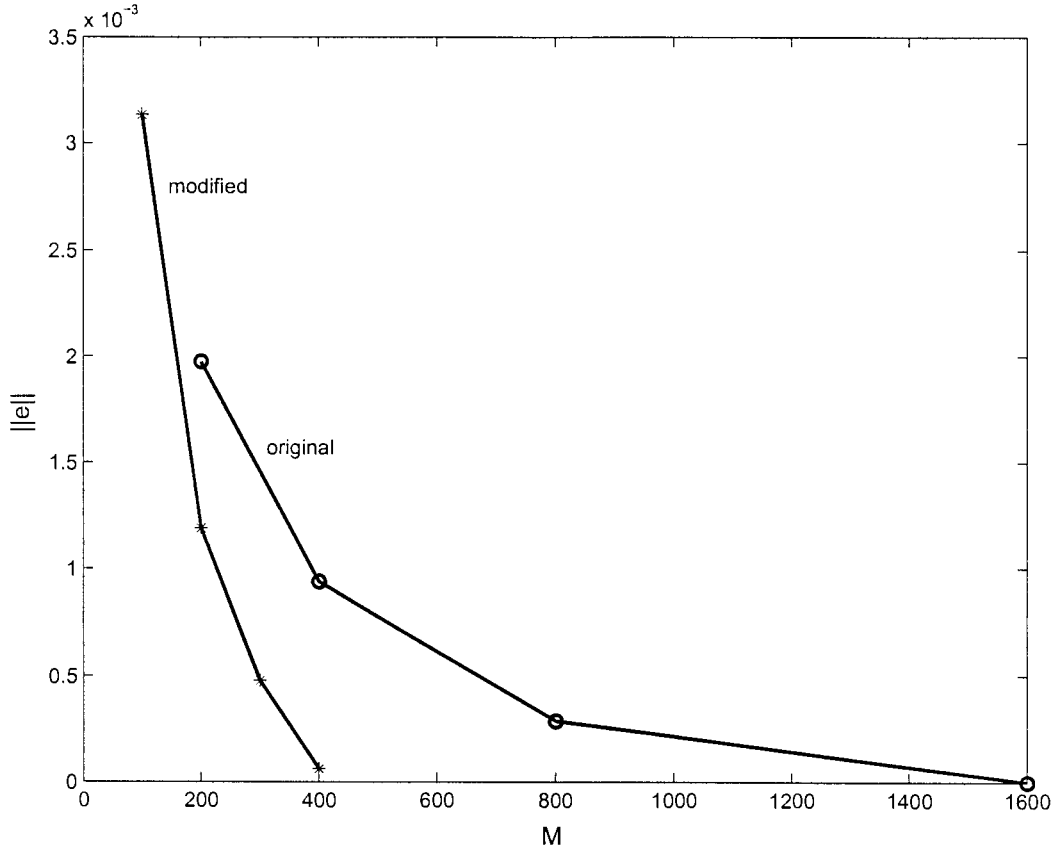
Figure 10. Convergence rates for the original and modified numerical schemes, $\epsilon = 0{\cdot}1$, $\nu = 0{\cdot}1$.

5. Conclusions

In this paper we have studied the indentation of a linear homogeneous isotropic elastic layer by a rigid cylindrical flat ended indenter. We have presented asymptotic analysis, approximate analytical solutions as well as numerical solutions using two different schemes. We have exhibited that the modified numerical scheme, in which we incorporate the approximate analytical solutions, provides us with accurate answers in coarser meshes. In particular, in terms of CPU time, using the modified scheme we get the same accuracy that we would get with the original scheme ten times faster. We have also justified the fact that we can use the approximate analytical solution to calculate the deformation gradient along the horizontal direction throughout the layer.

The method that we have presented has certain limitations. Its efficiency decreases when either ϵ or ν increase. Moreover, it provides us with an accurate analytical expression and an efficient way for calculating only the vertical component of the deformation field.

Another way to improve the numerical scheme would be to use an adaptive mesh in order to isolate the singularity. An adaptive mesh technique could be incorporated into either a finite elements or a finite-differences scheme. If one were to use an adaptive mesh with finite differences, some caution should be taken in order to maintain the second-order accuracy of the discretization (*i.e.* one would have to interpolate the numerically calculated solution between the ciarse and the fine mesh). Even in the case of an adaptive mesh, one could still subtract the

approximate analytical expressions in order to render the singularity milder. Thus, one could construct a modified numerical scheme, together with an adaptive mesh in order to improve the convergence rate even further. We have chosen to present this numerical/analytical method in a uniform mesh for illustrative purposes. We intend discuss the extension of this method for the case of an adaptive scheme in a later publication.

Another idea that this work suggests is that one could develop a finite-element code in which information concerning the structure of the solution (*i.e.* Equations 2.17a, 3.17b) is incorporated into the basis functions that are being used. In this way, the resulting problem has a 'milder' singularity and can be solved accurately in a coarser mesh. This approach has been used successfully in other cases of singularly perturbed systems [25] as well as in numerical homogenization [26].

Acknowledgments

References

1. J.R. Alblas and M. Kuipers, Contact problems of a rectangular block on an elastic layer of finite thickness Part I: The thin layer : Approximate analytic and numerical solutions for rigid flat indenters. *Acta Mechanica* 8 (1969) 133–145.
2. V.M. Aleksandrov, Asymptotic methods in contact problems of elasticity theory. *PMM* 32 (1968) 691–703.
3. V.M. Aleksandrov, Asymptotic solution of the contact problem for a thin elastic layer. *PMM* 33 (1969) 49–63.
4. V.M. Aleksandrov, V.A. Babeshko and V.A. Kucherov, Contact problems for an elastic layer of slight thickness. *PMM* 30 (1966) 148–172.
5. V.M. Aleksandrov and D.A. Pozharskii, *Nonclassical 3D Problems in the Mechanics of Contact Interaction of Elastic Bodies* (in Russian) Moscow: Factorial (1998) 288 pp.
6. V.M. Aleksandrov and I.I. Vorovich, Contact problems for the elastic layer of small thickness. *PMM* 28 (1964) 425–427.
7. G.M.L Gladwell. *Contact Problems in the Classical Theory of Elasticity*. Alphen aan den Rijn: Sijthoff and Noordhoff (1980) 716 pp.
8. W.C. Hayes, L.M. Keer, G. Herrmann and L.F. Mockros, A Mathematical Analysis for indentation tests of articular cartilage. *J. Biomech.* 5 (1972) 541–555.
9. K.L. Johnson, *Contact Mechanics*. Cambridge: Cambridge University Press (1985). 452 pp.
10. A.F. Mak, W.M. Lai and V.C. Mow, Biphasic indentation of articular cartilage-I. Theoretical Analysis. *J. Biomech.* 20 (1987) 703–714.
11. W.W. Gerberich, D.E. Kramer, N.I. Tymiak, A.A. Volinsky, D.F. Bahr and M.D. Kriese, Nanoindentation-induced defect-interface interactions: phenomena, methods and limitations. *Acta Mater.* 47 (1999) 4115–4123.
12. W. Yu and J.P. Blanchard, An elastic-plastic indentation model and its solutions. *J. Mat. Res.* 11 (1996) 2358–2367.
13. W.C. Bae, L.M. Lottman, L.R. Frank and R.L. Sah, Probe tip geomedegeneration. *Trans. Orthop. Res. Soc.* 25 (2000) 892–900.
14. M.H. Holmes and J. Bell, Model of the dynamics of receptor potential in a mechanoreceptor. *J. Biosci.* 110 (1992) 139–174.
15. I.N. Sneddon, *Mixed Boundary Value Problems in Potential Theory*. New York: Wiley (1966) 282 pp.
16. I.N. Sneddon, *Application of Integral Transforms in the Theory of Elasticity*. New York: Springer-Verlag (1976) 426 pp.

17. M. Sakamoto, G. Li, T. Hara and E. Chao, A new method for theoretical analysis of static indentation test. *J. Biomech.* 29 (1996) 679–685.

18. I.N. Sneddon, *The Use of Integral Transforms*. New York: McGraw-Hill (1972) 539 pp.

19. M.A. Haider, *Analytic Approximations for the Indentation of a Thin Layer Elastic Layer and a Viscoelastic Formulation in Finite Strain with Applications to the Mechanics of Biological Soft Issues.* PhD thesis, Rensselaer Polytechnic Institute (1996) 138 pp.

20. M.A. Haider and M.H. Holmes, A mathematical approximation for the solution of a static indentation test. *J. Biomech.* 30 (1997) 747–751.

21. M.A. Haider and M.H. Holmes, Identation of a thin compressible elastic layer: Approximate analytic and numerical solutions for rigid flat intenders. *J. Mech. Phys. Solids* 43 (1995) 1199–1219.

22. K.A. Atahnasiou, M.P. Rosenwasser, J.A. Buckwalter, T.I. Malinin and V.C. Mow, Interspecies comparisons of in situ intrinsic mechanical properties of distal femoral cartilage. *J. Orthopedic Res.* 9 (1991) 330–340.

23. J.R. Barber, *Elasticity*. Dordrecht: Kluwer Academic Publishers (1992) 292 pp.

24. L.C. Evans, *Partial Differential Equations.* Providence: AMS Publishers (1998) 662 pp.

25. S. Adjerid, M. Aiffa and J.E. Flaherty, Computational methods for singularly perturbed systems. *Proceedings of Symposia in Applid Mathematics* 56 (1999) pp. 47–83.

26. T.Y. Hou, X. Wou and Z. Cai, Convergence of a multiscale finite element method for elliptic problems with rapidly oscillating coefficients. *Math. Comp.* 68 (1999) 913–943.